

# Demosaicing of Periodic and Random Color Filter Arrays by Linear Anisotropic Diffusion

Jean-Baptiste Thomas<sup>^</sup> and Ivar Farup<sup>^</sup>

Department of Computer Science, NTNU – Norwegian University of Science and Technology, Teknologieveien 22,  
2815 Gjøvik, Norway  
E-mail: jean.b.thomas@ntnu.no

---

**Abstract.** *The authors develop several versions of the diffusion equation to demosaic color filter arrays of any kind. In particular, they compare isotropic versus anisotropic and linear versus non-linear formulations. Using these algorithms, they investigate the effect of mosaics on the resulting demosaiced images. They perform cross analysis on images, mosaics, and algorithms. They find that random mosaics do not perform the best with their algorithms, but rather pseudo-random mosaics give the best results. The Bayer mosaic also shows equivalent results to good pseudo-random mosaics in terms of peak signal-to-noise ratio but causes visual aliasing artifacts. The linear anisotropic diffusion method performs the best of the diffusion versions, at the level of state-of-the-art algorithms.*  
© 2018 Society for Imaging Science and Technology.  
[DOI: 10.2352/J.ImagingSci.Technol.2018.62.5.050401]

---

## 1. INTRODUCTION

Color image sensors usually capture images using spatio-spectral sampling based on a mosaic of primaries called a color filter array (CFA). It is important to reconstruct the spatial resolution of the image in order to display or store the data within a classical, standard, image representation (e.g., *a three-dimensional matrix*). In the case of custom primaries, a color transform to red, green, and blue (RGB) is also required for the same reasons.

The demosaicing of CFA is essentially an interpolation problem, which could take advantage of certain priors on natural image statistics. Indeed, spatial and/or spectral correlation is usually assumed for one specific object, and object edge estimates permit us to refine the assumptions. These aspects have led the color imaging community to develop many solutions, well summarized in [1–5]. Most solutions are dedicated to a single, specific mosaic, the Bayer pattern [6], which has very deep roots in signal theory (e.g., in respect of Shannon theorem) and in the understanding of the nature of color information (e.g., separability between luminance and chroma). It is unlikely that a new algorithm will break through independently of the optimization of the whole imaging pipeline—see the eloquent conclusion of the Li et al. survey [3]. We can note in particular the effect of

illumination [7], and of specific interest for this article, the role of the mosaic definition.

Indeed, older [8] and recent [9] studies have shown that a pseudo-random mosaic arrangement may improve the result of demosaicing. One of the reasons is that this redistributes noise in several frequencies, and thus reduces visible aliasing artifacts. Among the research in this direction, we can note that Condat [10] proposed algorithms to define random mosaic arrangements that exhibit blue noise characteristics of sampling, such that two adjacent pixels would be different primaries. Taking into account the practical issue for manufacturing random patterns, he also proposed a pseudo-random pattern, by tiling patterns while preserving their random properties. In [11], an optimal mosaic was proposed, but it was regular and used six primaries. Interest in a blue noise arrangement for mosaics comes from the model of retinal distribution of cones in the human eye, which is sometimes related to a blue noise type of distribution [10, 12]. In addition, according to the spatio-spectral correlation assumed by most demosaicing methods, specific patterns may help us to identify better edges to guide demosaicing, at the instar of the Bayer pattern.

However, random mosaics are not very easy to demosaic. Inverse distance weighted interpolation may be a potential candidate, but linear interpolation is unlikely to provide a robust result due to sparsity. Linear mean square error based demosaicing has been used successfully to demosaic pseudo-random patterns up to a certain size [9], but this concept is dependent on a training data set and may not be very accurate for large random structures. Variational models based on the diffusion equation have been used successfully in the demosaicing of random patterns, mostly using total variation (TV). Condat developed a TV framework for demosaicing [13, 14]. This is essentially non-linear isotropic diffusion. In his work, he investigated the results on several mosaics and showed that state-of-the-art results can be obtained with this solution, although not the best quantitative results. He also showed that more standard results can be obtained with patterns other than Bayer's. In his model, the luminance channel mostly drives the regularization, and chromaticity estimation may be affected. (Note: [13] is a preprint of [14] but contains useful extra information.) A version that includes denoising was also presented [15]. Saito and Komatsu [16, 17] developed a TV-based, isotropic, demosaicing algorithm for the Bayer

---

<sup>^</sup> IS&T Members.

Received Mar. 22, 2018; accepted for publication June 30, 2018; published online Oct. 15, 2018. Associate Editor: Masato Tsukada.  
1062-3701/2018/62(5)/050401/8/\$25.00

pattern on the R, G, and B channels. They followed up with an improved version that couples R and B channels to the G channel [18, 19], which removes artifacts at edges. They developed a more advanced coupling of the channels in a subsequent article [20], which provides good visual results. Variational frameworks have also been proposed for demosaicing spectral filter arrays (SFA) [21].

All of the variational approaches listed above are isotropic (the effective diffusion coefficient is a scalar, not a tensor) and non-linear (the effective diffusion coefficient is a function of the final demosaiced image). The mentioned research evaluates the results of the proposed non-linear isotropic algorithms on a data set versus the state of the art, but there has been little investigation on the fundamental modalities of the diffusion equation developed besides the proposal. Linear and/or anisotropic methods, to the best of our knowledge, have not been tested for demosaicing. In addition, the fundamental characteristics of the mosaics are not compared deeply.

In this article, we propose to develop the investigation of several diffusion equation derivations, isotropic versus anisotropic and linear versus non-linear, jointly with several patterns based on random noise of several chromatic characteristics (blue, white, pink). The results are evaluated based on linear regression analysis and are also compared with the state of the art using paired statistical tests. We demonstrate that the linear anisotropic diffusion performed on color channels and combined with the pseudo-random mosaic identified by Amba et al. [9] gives the best visual results with peak signal-to-noise ratio (PSNR), competitive with the state of the art.

## 2. DIFFUSION METHODS FOR DEMOSAICING

We develop a demosaicing algorithm inspired by the works by Condat [14] and Saito and Komatsu [20]. It follows their approach in that a version of the diffusion equation is used. However, instead of limiting the approach to isotropic non-linear diffusion, we make a general framework that gives the flexibility to use all possible combinations of isotropic and anisotropic, linear and non-linear diffusion.

Let  $\Omega \subset \mathbb{R}^2$  denote the image domain and  $M^c \subset \Omega$  denote the subset of the image domain that is covered by the sensor mosaic of channel  $c \in \{R, G, B\}$ . In each pixel, only one of the channels is present, so  $\bigcap_c M^c = \emptyset$ . Most often, all pixels are represented in one channel such that  $\bigcup_c M^c = \Omega$ , but actually, neither of these conditions is strictly necessary for the proposed method. The pixel values of the mosaiced image are denoted by  $u_M^c(x)$  for  $x \in M^c$ . The task of the demosaicing algorithm is to find the values for all the pixels in the image,  $u^c(x)$  for  $x \in \Omega$ , such that  $u^c(x) = u_M^c(x)$  for  $x \in M^c$ . In other words, we limit the treatment here to pure demosaicing, leaving out combined demosaicing and denoising.

A simple approach is to assume that the image channels are smooth, i.e., the image has a strong spatial correlation.

This can be achieved, e.g., by minimizing the functional

$$E(u) = \int_{\Omega} \|\nabla u\|^2 dA, \quad (1)$$

where  $\|\cdot\|$  denotes the Frobenius norm over three image channels and two spatial dimensions of the gradient. This leads to a constrained Poisson problem

$$\nabla^2 u^c = 0, \quad x \in \Omega \setminus M^c \quad (2)$$

$$u^c = u_M^c, \quad x \in M^c, \quad (3)$$

which can be solved by gradient descent

$$\frac{\partial u^c}{\partial t} = \nabla^2 u^c, \quad (4)$$

with symmetric boundary conditions. We discretize this equation using a forward Euler finite difference scheme for the time derivative, a centered finite difference scheme for the Laplacian, and denote the final solution as  $u_P$  (indicating Poisson).

There are at least two problems with the Poisson solution  $u_P$ . First, it will not preserve edges very well. Second, there is no coupling between channels, so there is no guarantee that small details and edges will occur at the same pixel position in different color channels. In order to handle this, we introduce the  $2 \times 2$  structure tensor of the image defined in each position of the image [22]:

$$S(u) = \begin{pmatrix} \sum_c \left( \frac{\partial u^c}{\partial x} \right)^2 & \sum_c \frac{\partial u^c}{\partial x} \frac{\partial u^c}{\partial y} \\ \sum_c \frac{\partial u^c}{\partial x} \frac{\partial u^c}{\partial y} & \sum_c \left( \frac{\partial u^c}{\partial y} \right)^2 \end{pmatrix}. \quad (5)$$

Let  $\lambda_+$  and  $\lambda_-$  denote the eigenvalues of the structure tensor. A local diffusion coefficient inspired by Perona and Malik [23] can then be defined as

$$d(\lambda_+) = \frac{1}{1 + \kappa \lambda_+^2}, \quad (6)$$

where  $\kappa$  is a suitably chosen constant, and used for *isotropic diffusion*,

$$\frac{\partial u^c}{\partial t} = \nabla \cdot (d(\lambda_+) \nabla u^c). \quad (7)$$

We denote the solutions of this equation by  $u_i$  (indicating isotropy).

In order to obtain anisotropic diffusion, let  $E$  be the matrix with the eigenvectors of the structure tensor corresponding to the eigenvectors  $\lambda_{\pm}$  as columns. The structure tensor can then be written as  $S = E^T \text{diag}(\lambda_+, \lambda_-) E$ . Following Sapiro and Ringach [24], we define the diffusion tensor as

$$D = E^T \text{diag}(d(\lambda_+), d(\lambda_-)) E. \quad (8)$$

The corresponding *anisotropic diffusion* equation is [24]

$$\frac{\partial u^c}{\partial t} = \nabla \cdot (D \nabla u^c). \quad (9)$$

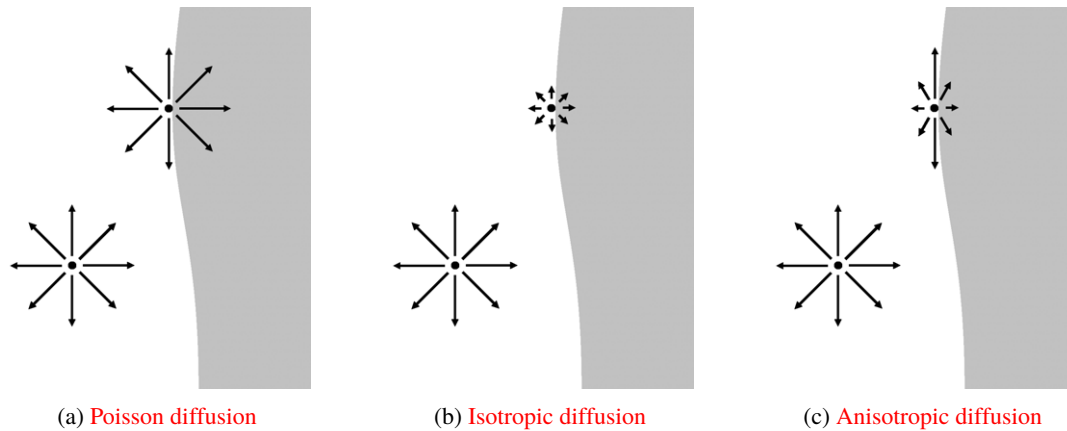


Figure 1. Illustration of the effect of the behavior of the three different diffusion methods close to an edge in an image.

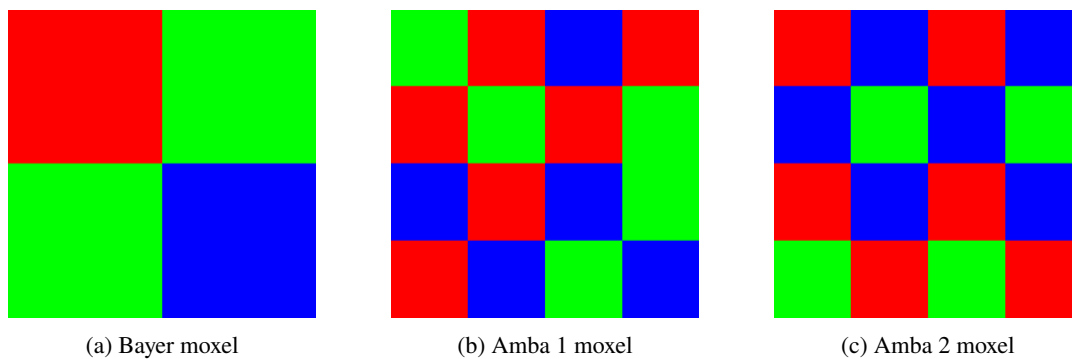


Figure 2. Moxels of the regular and pseudo-random mosaics used.

We denote the solutions of this equation by  $u_a$  (indicating anisotropy).

As in the Poisson case, both the isotropic (7) and anisotropic (9) diffusion equations can be solved by a forward Euler finite difference method. The gradient and divergence are discretized with forward and backward finite differences, respectively. As an initial value, we use the result of the simple Poisson demosaicing described above,  $u_p$ . An illustration of the effect of the three different diffusion schemes is shown in Figure 1.

For the structure tensor, from which the diffusion coefficient and diffusion tensor are defined, we have two principally different options. Either it can be defined in terms of the initial Poisson solution,  $S(u_p)$ , or it can be taken as a function of the final demosaiced image,  $S(u)$ . The former will give rise to a linear problem, whereas the latter will give rise to a non-linear one. Thus, in total, we now have four principally different solutions of the demosaicing problem, corresponding to the choices of isotropic versus anisotropic and linear versus non-linear, respectively. In all of these methods, channel coupling is introduced by means of the structure tensor (5). Thus, the channels are coupled through the Euclidean distance in the sensor RGB space, which will include lightness, chroma, and hue differences. It should be

noted that all methods cited in the introduction would in principle be very similar to isotropic non-linear diffusion.

### 3. EXPERIMENTAL PROTOCOL

We describe here the details of procedures for the mosaic creations, selection of image set, demosaicing methods, and parameters selected for the quantitative investigation.

#### 3.1 Mosaics

Bayer mosaic has been selected as per reference to the state of the art. Its mosaic element (moxel) is shown in Figure 2(a). We also selected the best pseudo-random mosaics from Amba et al. [9], for which moxels are shown in Fig. 2(b) and (c). Those moxels are repeated until they fit the size of the images. We did not investigate other regular or pseudo-random mosaics because we decided to follow the selection of mosaics performed by Amba et al. [9]. We also limited the investigation to  $R, G, B$  moxels, excluding more than three primaries or complementary filters. We, however, selected unconstrained random mosaics because the spatial frequency properties of the mosaics impact image reconstruction, e.g., spatial aggregation of similar filters may help us to better evaluate local gradients.

We decided to implement a simple noise model of mosaic based on frequency filtering. Random mosaics have

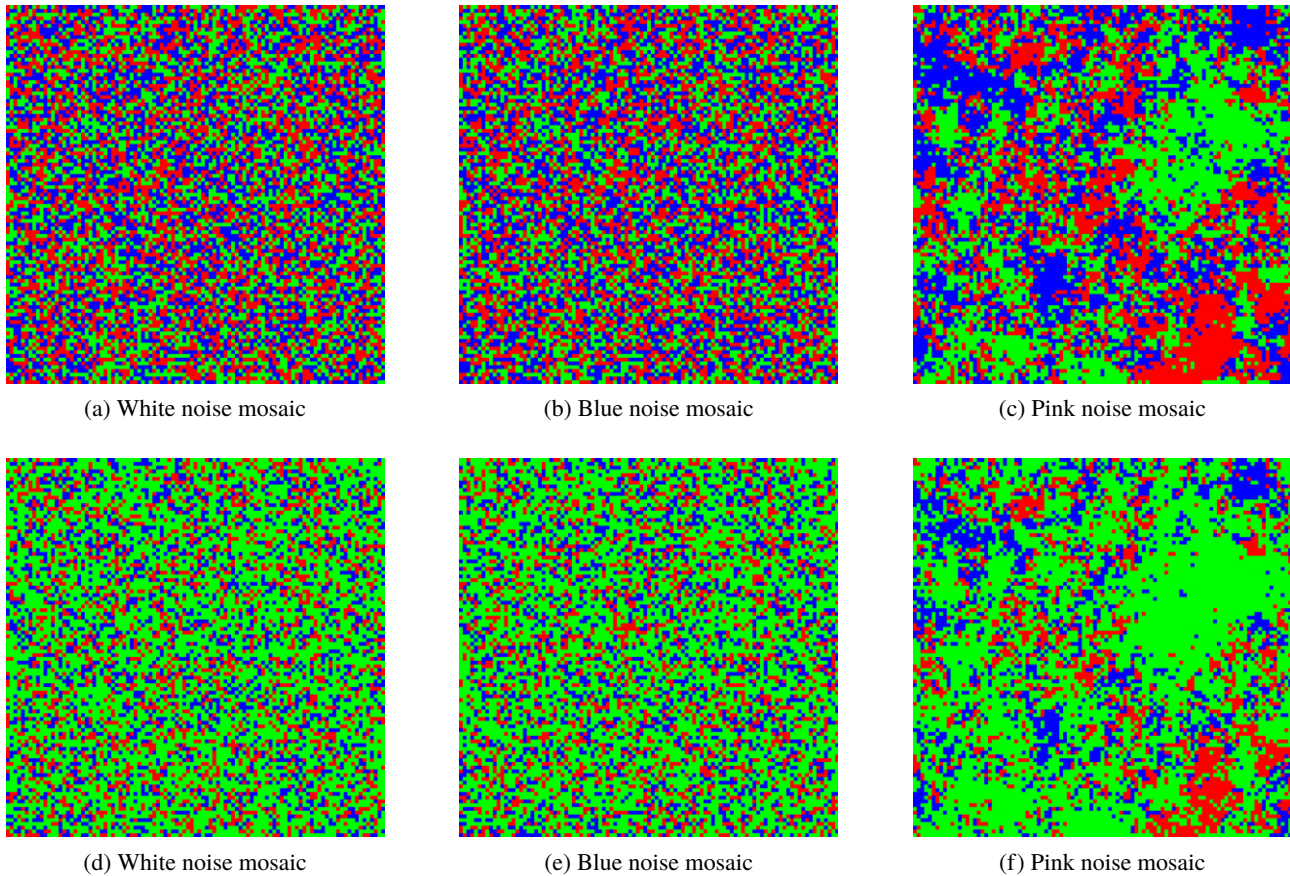


**Figure 3.**  $100 \times 100$  center pixels of the random mosaics. Top line: It visually seems that there are more green pixels, but the count is equivalent in these three distributions. Little differences are observed between the blue noise and the white noise, which is confirmed by a frequency analysis. Bottom line: Random mosaics with an oversampled green channel. We observed a sparser occurrence of red and blue pixels, which would permit, in principle, generating a better gradient map while using the green channel.

been created by frequency filtering of a white noise of three intensity “images” (we used the MATLAB function *randnd()* from Marcin Konowalczyk [25]), followed by a maximum-based selection for which a channel is sampled at one location so that there are no empty pixels in the mosaic. With this strategy, we generated approximated white, pink and blue noise mosaics as shown in Figure 3(a)–(c).

We also generated an oversampled green version of those mosaics by multiplying the intensity of the green random image by 2 before the maximum-based selection. This leads to a distribution of green slightly more than double that of the other two components. Those mosaics are shown in Fig. 3(d)–(f).

All the mosaics are generated by the same random seed, and only once, to avoid instability of results during the comparison, but we ensured visually that they were representative. They are adjusted to the image from the center, so the large part of the sampling remains the same across images of the databases. We did a frequency analysis similar to what was performed by Alleysson et al. [26] and verified that the pink noise was reasonably pink and the white noise was white; however, it was really difficult to assess the blue noise. The blue noise version we generated is very close

to a white noise, and this is verified in the results later, where the blue and white noise mosaics exhibit similar results, with a little advantage for the white noise. Nevertheless, the two-dimensional blue noise generation is still an open problem, and we accepted this instance as representative enough for this work.

Increasing green channels or having pink noise patterns creates chromatic blotches in which one specific channel is sampled at the sensor resolution, which may help edge identification while assuming strong spectral correlation.

### 3.2 Images

The imaging process is simulated based on these mosaics and on the commonly used color image data sets: Kodak [27] and IMAX [28]. Kodak has been used for decades as the benchmark for demosaicing fields, although some literature says that it is not very well representative of the real world. In particular, it does not contain very high saturation and high intensity edges (see e.g., [3]), compared to what is achieved by modern cameras. It is accepted that most demosaicing would perform well on this database, but the fence part of the lighthouse image is a very good example of the aliasing effect. IMAX is a more recent benchmark set, which is known to be more challenging due to higher saturation and hue

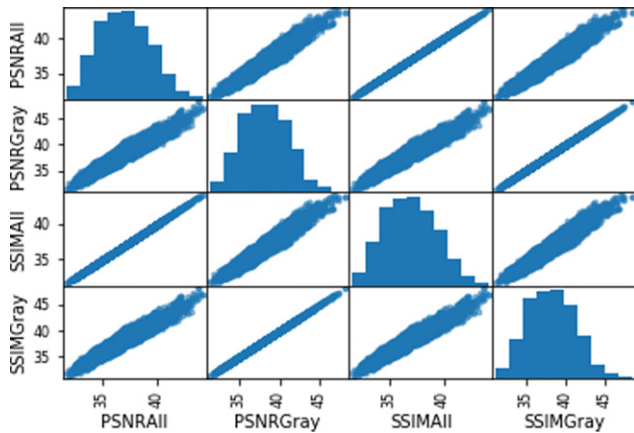


Figure 4. Correlation between PSNR and SSIM indicates that we can use one of them in the following. PSNRAll stands for the color PSNR description and PSNRGray stands for a PSNR estimated on a graylevel image version computed as a weighted linear sum of the R, G, and B channels as in sRGB.

complexity, but also more representative of what is captured with modern cameras. Thus, we consider these image sets to be complementary and have used both of them.

### 3.3 Demosaicing

As a preliminary experiment, we ran the pure Poisson solver (4) on all images and mosaics described above. However, the results were clearly visually poorer than other recent methods, so the resulting images were not included in the final analysis below.

We also tried coupling the channels only through the lightness channel  $u^L$  computed as a weighted average of the RGB color channels. In this case, the eigenvalues of the structure tensor simply become  $\lambda_+ = |\nabla u^L|$  and  $\lambda_- = 0$ , and the corresponding eigenvectors will be directed parallel and orthogonal to the gradient  $\nabla u^L$ , respectively. Used with the isotropic (7) and anisotropic (9) schemes, this gave visually quite good results. However, a statistical analysis on the PSNR from these preliminary experiments quickly showed that it could not compete with using the full color structure tensor (5).

We further tried adding a blurring convolution mask as a preprocessing step before computing the structure tensor (5), without any measurable effect. This is probably because the image resulting from the first Poisson solver is already somewhat blurred.

Thus, we decided to focus our analysis on the behavior of the method using isotropic (7) versus anisotropic (9) diffusion with a full RGB color structure tensor (5), linear  $S(u_p)$  versus non-linear  $S(u)$  diffusion, and various values of  $\kappa \in \{10^2, 10^3, 10^4\}$  across all mosaics and images described above.

## 4. ANALYSIS

We analyze the behavior of the developed algorithm across different images, mosaics, and parameters, and against a state-of-the-art method.

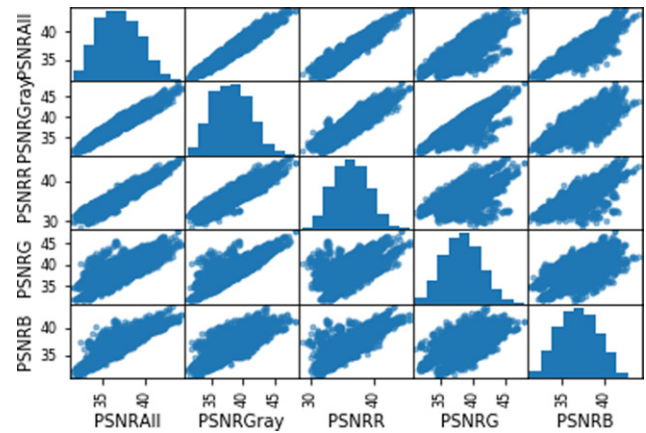


Figure 5. Correlation between PSNRs of different channels indicates that we can use only PSNRAll in the following. PSNRAll stands for the color PSNR description and PSNRGray stands for a PSNR estimated on a graylevel image version computed as a weighted linear sum of the R, G, and B channels as in sRGB. PSNRR, PSNRG, and PSNRB stand for the PSNR computed on the mentioned color channel. Similar results are obtained for SSIM.

### 4.1 Quality Measure

It is common practice in the demosaicing literature to measure the performance of the demosaicing algorithm by comparing the demosaiced images with a ground truth by means of PSNR. Since the PSNR does not necessarily correlate very well with perceptual correspondence between the images, perceptual image difference metrics like structural similarity (SSIM) [29] can be used. Figure 4 shows a scatter matrix plot of PSNR and SSIM computed for all the test images using all channels and only the luminance channel. Since the correlation between SSIM and PSNR is much higher than the correlation between all channels and the luminance channel only, there is no reason to go beyond the simpler PSNR for the following analysis.

A similar analysis between PSNR values computed across all channels, on the luminance channel and the individual channels, respectively, is shown in Figure 5. For the PSNR gray versus individual channels, the correlation reproduces the weights of the RGB to grayscale transformation. On average, the correlation is smallest with the green channel. For some reason there is higher correlation between red and blue than between any of them and green. This could be due to the fact that many of the images are computed with the double green mosaics.

Based on this analysis, we find it reasonable to use the PSNR computed across all channels as a quality measure for the demosaicing algorithms in the following analysis.

### 4.2 Mosaics

In order to compare the behavior of the algorithms for various mosaics, we perform an ordinary least squares regression analysis, fitting the PSNR to the mosaics across all the images and algorithms and computing the  $p$ -values and linear regression slopes. We observe that the Amba1, Amba2, and Bayer mosaics perform the best overall, and clearly better than all of the random mosaics. Surprisingly, the single green

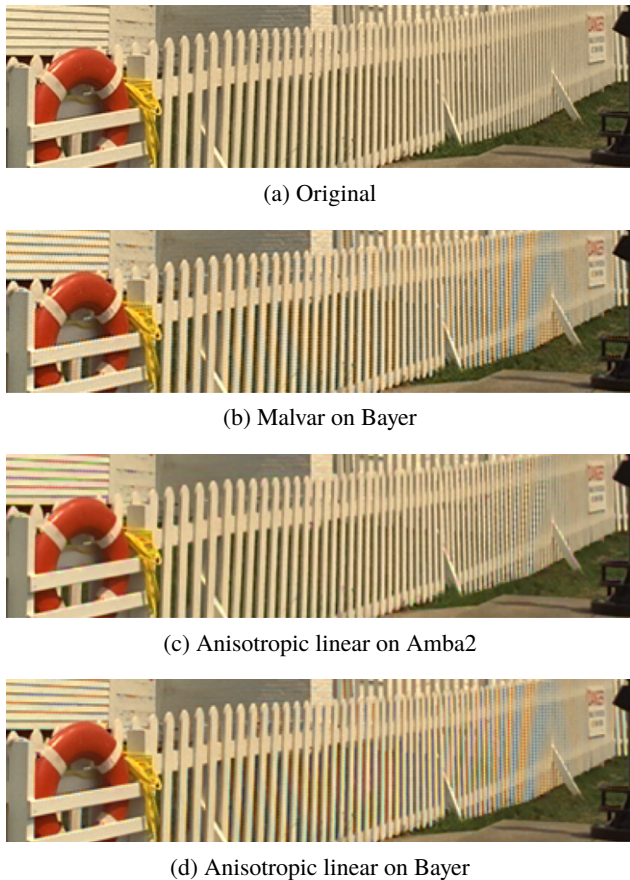


**Figure 6.** Crop of lighthouse image (Kodim19). We observe that the aliasing artifact is generated strongly by the Bayer moxel for both demosaicing algorithms, compared to the Amba2 moxel. Malvar exhibits some zipping visible in particular on the wooden wall above the buoy. This area is prone to chromatic artifacts with all methods. However, edges of the buoy seem slightly better preserved with the Bayer moxel. For the anisotropic method on Amba2, we also observe a reddish and bluish halo around the dark object occluding the fence on the right. This could be explained by the predominance of red and blue filters in the moxel.

versions of the random mosaics consistently perform better than the double green versions for all the noise types. This may be caused by the computation of the structure tensor from the original Poisson solution,  $u_p$ , which does not benefit from the oversampling of a specific channel for the definition of edges. The pink noise mosaics show lower performance than the other random mosaics.

In order to get even more refined results among the better mosaics, we perform the paired sign test (binomial test of the sign of the difference of the PSNRs) for pairs of mosaics across all images and algorithms. This showed that Amba2 is significantly better than Amba1 ( $p < 10^{-4}$ ) and Amba2 is significantly better than Bayer ( $p < 10^{-4}$ ), whereas there is no significant difference between Amba1 and Bayer ( $p = 0.7$ ). This analysis was also repeated for the anisotropic diffusion method alone, with the same result: Amba2 is better than Amba1 and Bayer, and there is no significant difference between Amba1 and Bayer.

### 4.3 Methods

Like for the mosaics, an ordinary least squares regression analysis is performed to analyze the behavior of the methods: linear versus non-linear and isotropic versus anisotropic. It is clear from the regression analysis that anisotropic diffusion outperforms the isotropic formulation. Also, linear tends to perform better than non-linear diffusion. These trends are confirmed by the sign tests:

- Anisotropic performs significantly better than isotropic diffusion across all methods, mosaics, and images ( $p < 10^{-4}$ ). The average difference between anisotropic and isotropic diffusion is a PSNR of 0.86 dB.
- Linear performs significantly better than non-linear diffusion across all methods, mosaics, and images ( $p < 10^{-4}$ ), but the effect is very small: an average difference in PSNR of 0.08 dB.
- Linear performs significantly better than non-linear diffusion for both isotropic diffusion and anisotropic diffusion across all mosaics and images ( $p < 10^{-4}$  and  $p = 0.0002$ , respectively).

The difference between linear and non-linear is very small but, surprisingly, in favor of linear diffusion. This result is quite fortunate since linear diffusion is much less computationally expensive than non-linear diffusion. By means of ordinary least squares regression, we also investigated whether the isotropic methods were particularly accurate for any given mosaic, but we found no significant cross-effects between the methods and the mosaics.

Ordinary least squares regression on PSNR versus  $\kappa$  across all the diffusion methods showed a strong correlation ( $p = 0.007$  for the slope being different from zero) with increasing performance, with increasing  $\kappa$  value. Thus, the best results correspond to  $\kappa = 10^4$ .

### 4.4 Images and Database

Regression analysis on the entire PSNR result data set shows that most of the variation in the data set comes from the difference in the images ( $R^2 = 0.658$ ). Since there is such a strong dependence on the images, it is interesting to see if there is a big difference between the Kodak and IMAX image sets. Regression shows that there is no significant dependence on the data set ( $p = 0.148$ ).

### 4.5 Comparison with State of the Art

We compared the proposed algorithms with the method from Malvar et al. [30] on the Bayer mosaic as a representative of the state of the art. Although this may not be the best performing method in terms of peak performance, it shows stable results at the level of the state of the art and is well established (implemented in MATLAB). Since state-of-the-art methods are usually applicable only to the Bayer mosaic, except a few (Lukac, Condat, Amba, etc.), it is relevant to analyze the behavior of our proposed method on this particular mosaic. A paired sign test does not detect a statistically significant difference between the proposed linear anisotropic diffusion (with  $\kappa = 10^4$ ) and the Malvar

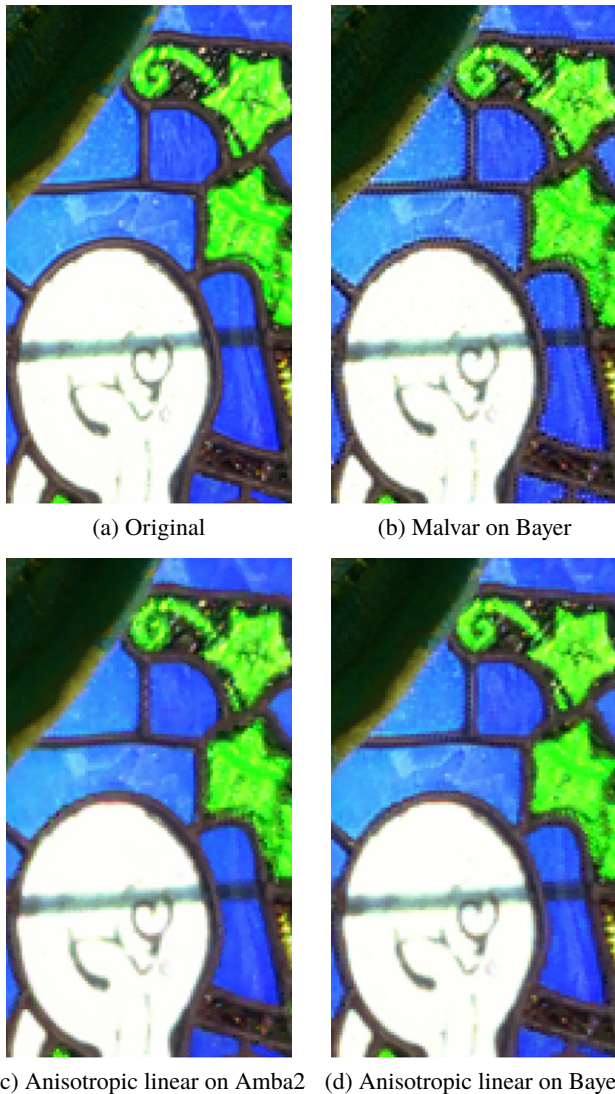


Figure 7. Crop of the first image of the IMAX data (IMAX01). Minimum artifacts are generated by the algorithms on the edges between the white glass and the dark holders. Yet, Malvar exhibits more zipping on these edges compared to the linear anisotropic method. On the contrary, it seems that the edges are a little blurred and slightly chromatic with the linear anisotropic method. If we look at the curtain on the top left, Malvar exhibits a strong zipping.

algorithm ( $p = 0.088$  with a PSNR difference of 0.22, in favor of the proposed method). However, the linear anisotropic diffusion method with the Amba2 mosaic (average PSNR of 38.99) performs significantly better than Malvar on the Bayer mosaic (average PSNR of 38.87), but the differences are small.

#### 4.6 Visual Observations

Overall, we observed that the linear anisotropic method on Amba2 performed visually better on most images. In general, the random noise mosaics do not give very stable results and some regions could be very good while some exhibit strong artifacts. We thus deduce that a carefully chosen pseudo-random is more efficient than fully random instances. In

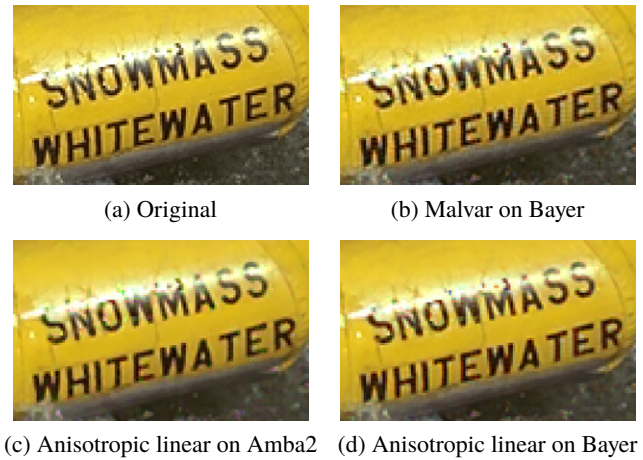


Figure 8. Crop of the rafting boat image (Kodim 14). We observe a better reconstruction of the text with the linear anisotropic method on Amba2 mosaic. Both algorithms are equivalent on the Bayer mosaic.

Figures 6–8, we illustrate some specific behavior. Captions provide more specific analysis of the images.

## 5. CONCLUSION

A diffusion-based demosaicing algorithm has been developed in different versions and tested on different periodic and random mosaics. It was found that anisotropic diffusion works better than isotropic diffusion, and that linear worked somewhat better than non-linear diffusion, and is also computationally less expensive. Comparing the mosaics, we found that the periodic mosaics performed better than all the random mosaics with different noise types both with and without double sampling of the green channel. Linear anisotropic diffusion performed at the same level as Malvar's state-of-the-art algorithm on the Bayer mosaic, and significantly better on the Amba2 mosaic.

Direct extensions include the use of perceptual color metrics for the coupling of channels and psychometric quality evaluation compared to the best state-of-the-art methods. This class of algorithms could also be generalized to spectral filter arrays of any dimension and any mosaic design. Also, a global model of imaging pipeline could be derived and include demosaicing, denoising, and super-resolution together based on a similar formulation.

## REFERENCES

- 1 R. Ramanath, W. E. Snyder, G. L. Bilbro, and W. A. Sander III, "Demosaicing methods for Bayer color arrays," *J. Electron. Imaging* **11**, 306–315 (2002).
- 2 B. K. Gunturk, J. Glotzbach, Y. Altunbasak, R. W. Schafer, and R. M. Mersereau, "Demosaicing: color filter array interpolation," *Signal Process. Mag.* **22**, 44–54 (2005).
- 3 X. Li, B. Gunturk, and L. Zhang, "Image demosaicing: a systematic survey," in *Visual Communications and Image Processing*, edited by W. A. Pearlman, J. W. Woods, and L. Lu (SPIE, Bellingham, WA, 2008), Vol. 6822.
- 4 O. Losson, L. Macaire, and Y. Yang, "Comparison of color demosaicing methods," in *Advances in Imaging and Electron Physics*, edited by P. Hawkes (Elsevier, New York, NY, 2010), Vol. 162, pp. 173–265, chapter 5.

- <sup>5</sup> D. Menon and G. Calvagno, "Color image demosaicking: An overview," *Image Commun.* **26**, 518–533 (2011).
- <sup>6</sup> B. E. Bayer, "Color imaging array." US Patent 3,971,065 (1976).
- <sup>7</sup> S. Mihoubi, B. Mathon, J.-B. Thomas, O. Losson, and L. Macaire, "Illumination-robust multispectral demosaicking," *The six IEEE Int'l. Conf. on Image Processing Theory, Tools and Applications IPTA* (IEEE, Piscataway, NJ, 2017).
- <sup>8</sup> W. Zhu, K. Parker, and M. A. Kriss, "Color filter arrays based on mutually exclusive blue noise patterns," *J. Vis. Commun. Image Represent.* **10**, 245–267 (1999).
- <sup>9</sup> P. Amba, J. Dias, and D. Alleysson, "Random color filter arrays are better than regular ones," *J. Imaging Sci. Technol.* **60**, 50406 (2016).
- <sup>10</sup> L. Condat, "Color filter array design using random patterns with blue noise chromatic spectra," *Image Vis. Comput.* **28**, 1196–1202 (2010).
- <sup>11</sup> L. Condat, "A new color filter array with optimal sensing properties," *16th IEEE Int'l. Conf. on Image Processing (ICIP)* (IEEE, Piscataway, NJ, 2009), pp. 457–460.
- <sup>12</sup> J. Yellott, "Spectral consequences of photoreceptor sampling in the rhesus retina," *Science* **221**, 382–385 (1983).
- <sup>13</sup> L. Condat, A generic variational framework for demosaicking and performance analysis of color filter arrays. Working paper or preprint, April 2008.
- <sup>14</sup> L. Condat, "A generic variational approach for demosaicking from an arbitrary color filter array," *16th IEEE Int'l. Conf. on Image Processing (ICIP)* (IEEE, Piscataway, NJ, 2009), pp. 1625–1628.
- <sup>15</sup> L. Condat and S. Mosaddegh, "Joint demosaicking and denoising by total variation minimization," *19th IEEE Int'l. Conf. on Image Processing* (IEEE, Piscataway, NJ, 2012), pp. 2781–2784.
- <sup>16</sup> T. Saito and T. Komatsu, "Super-resolution sharpening-demosaicking with spatially adaptive total-variation image regularization," in *Advances in Multimedia Information Processing - PCM 2005*, edited by Y.-S. Ho and H. J. Kim (Springer, Berlin, Heidelberg, 2005), pp. 246–256.
- <sup>17</sup> T. Komatsu and T. Saito, "Spatially adaptive super-resolution sharpening-demosaicking for a single solid-state color image sensor," *Proc. SPIE* **6069**, 6069 (2006).
- <sup>18</sup> T. Saito and T. Komatsu, "Demosaicking method using the extended color total-variation regularization," *Proc. SPIE* **6817**, 68170C (2008).
- <sup>19</sup> T. Saito and T. Komatsu, "Demosaicking approach based on extended color total-variation regularization," *15th IEEE Int'l. Conf. on Image Processing* (IEEE, Piscataway, NJ, 2008), pp. 885–888.
- <sup>20</sup> T. Saito, Y. Takagaki, and T. Komatsu, "Three kinds of color total-variation semi-norms and its application to color-image denoising," *18th IEEE Int'l. Conf. on Image Processing* (IEEE, Piscataway, NJ, 2011), pp. 1457–1460.
- <sup>21</sup> K. Shinoda, T. Hamasaki, M. Kawase, M. Hasegawa, and S. Kato, "Demosaicking for multispectral images based on vectorial total variation," *Opt. Rev.* **23**, 559–570 (2016).
- <sup>22</sup> S. Di Zenzo, "A note on the gradient of a multi-image," *Comput. Vis. Graph. Image Process.* **33**, 116–125 (1986).
- <sup>23</sup> P. Perona and J. Malik, "Scale-space and edge detection using anisotropic diffusion," *IEEE Trans. Pattern Anal. Mach. Intell.* **12**, 629–639 (1990).
- <sup>24</sup> G. Sapiro and D. L. Ringach, "Anisotropic diffusion of multivalued images with applications to color filtering," *IEEE Trans. Image Process.* **5**, 1582–1586 (1996).
- <sup>25</sup> Code for the noise frequency filtering. [https://se.mathworks.com/matlabcentral/fileexchange/59305-randnd?s\\_tid=prof\\_contriblnk](https://se.mathworks.com/matlabcentral/fileexchange/59305-randnd?s_tid=prof_contriblnk) Accessed: 2017-03-22.
- <sup>26</sup> D. Alleysson, S. Susstrunk, and J. Herault, "Linear demosaicking inspired by the human visual system," *IEEE Trans. Image Process.* **14**, 439–449 (2005).
- <sup>27</sup> Kodak image database. <http://r0k.us/graphics/kodak/> Accessed: 2017-01-18.
- <sup>28</sup> L. Zhang, X. Wu, A. Buades, and X. Li, "Color demosaicking by local directional interpolation and nonlocal adaptive thresholding," *J. Electron. Imaging* **20**, 023016 (2011).
- <sup>29</sup> Z. Wang, A. C. Bovik, H. R. Sheikh, and E. P. Simoncelli, "Image quality assessment: from error visibility to structural similarity," *IEEE Trans. Image Process.* **13**, 600–612 (2004).
- <sup>30</sup> R. Malvar, L. He, and R. Cutler, "High-quality linear interpolation for demosaicing of Bayer-patterned color images," *Int'l. Conf. of Acoustic, Speech and Signal Processing* (IEEE, Piscataway, NJ, 2004).